JFM RAPIDS
journals.cambridge.org/rapids

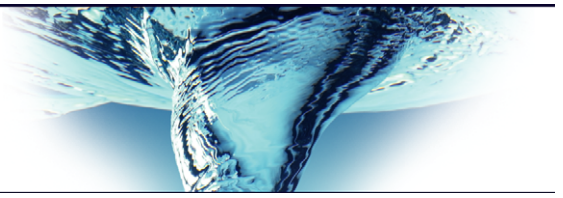

Transient dynamics by continuous-spectrum perturbations in stratified shear flows

R. Camassa and C. Viotti†

Carolina Center for Interdisciplinary Applied Mathematics, Department of Mathematics, University of North Carolina, Chapel Hill, NC 27599, USA

(Received 12 November 2012; revised 20 December 2012; accepted 4 January 2013; first published online 7 February 2013)

The transient dynamics of the linearized Euler–Boussinesq equations governing parallel stratified shear flows is presented and analysed. Solutions are expressed as integral superpositions of generalized eigenfunctions associated with the continuous-spectrum component of the Taylor–Goldstein linear stability operator, and reveal intrinsic dynamics not captured by its discrete-spectrum counterpart. It is shown how continuous-spectrum perturbations are generally characterized by non-normal energy growth and decay with algebraic asymptotic behaviour in either time or space. This behaviour is captured by explicit long-time/far-field expressions from rigorous asymptotic analysis, and it is illustrated with direct numerical simulations of the whole (non-Boussinesq) stratified Euler system. These results can be helpful in understanding recent numerical observations for parallel and non-parallel perturbed stratified shear flows.

Key words: geophysical and geological flows, instability, stratified flows

1. Introduction

Recent numerical simulations (Camassa & Viotti 2012) have shown that stratified shear layers induced by large-amplitude internal gravity waves can effectively remove small perturbations in the path of these waves, depleting the perturbation energy and absorbing it into the wave's background flow. Such depletion is stronger in the core region of the shear, and appears as a characteristic 'filamentation' of the perturbation pattern. Remarkably, such a scenario persists even when the Richardson number of the shear flow falls below its critical threshold, $Ri < 1/4$, whereupon instability evolving into Kelvin–Helmholtz roll-ups can be expected to develop. Previous studies (Farrel & Ioannou 1993) in the simple setup of linear stratification have provided evidence that neutrally-stable, parallel stratified shear layers can deplete small perturbations in a similar fashion. This effective damping by filamentation can in fact already be observed in the simpler setting of parallel, stratified shear Euler flows. An example

† Email address for correspondence: claudio.viotti@ucd.ie

doi:10.1017/jfm.2013.19

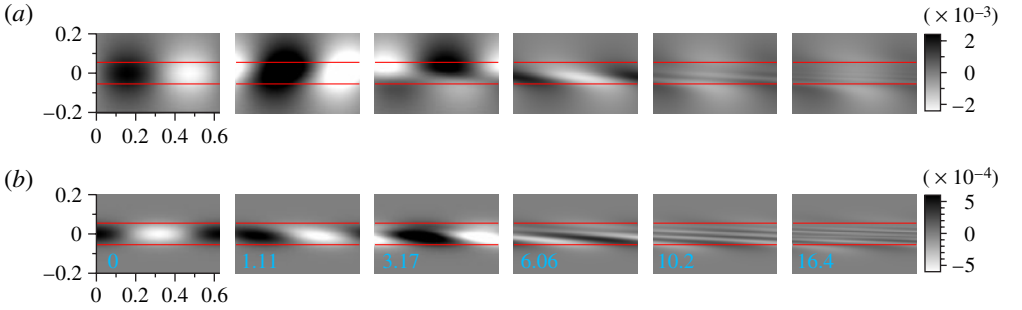

FIGURE 1. Vertical velocity perturbation (a) and density perturbation (b) from parallel shear simulation of the full Euler system (i.e. no Boussinesq approximation) with the numerical algorithm 'VARDEN' (Almgren *et al.* 1998). Horizontal lines reference the 10 % and 90 % background density variation levels; times are shown in (b). The shear is neutrally stable for the parameters of this example (in SI units): $U_0 = 0$, $\mathscr{U} = -0.1$, $\rho_1 = 1$, $\rho_2 = 1.02$, $\delta = 0.05$, $k = 10$, $L = 3\lambda_x/4 = 3\pi/(2k)$ and $g = 9.8$. Resolution on a square grid is $L/512$, with computational domain corresponding to one perturbation period.

from a direct numerical simulation of the Euler equations

$$(\rho \boldsymbol{u})_t + (\boldsymbol{u}\cdot\nabla)(\rho\boldsymbol{u}) = -\nabla p - g\rho \boldsymbol{y}, \quad \rho_t + \boldsymbol{u}\cdot\nabla\rho = 0, \quad \nabla\cdot\boldsymbol{u} = 0, \tag{1.1}$$

for the two-dimensional velocity field $\boldsymbol{u}(\boldsymbol{x}, t)$ and density $\rho(\boldsymbol{x}, t)$ of a fluid confined between two rigid plates at $\boldsymbol{x} = (x, y)$, $-L < y < L$, subject to gravity g, illustrates this behaviour (see figure 1). As one can see, an initial condition obtained by superimposing a first baroclinic mode $\boldsymbol{u}' = \hat{\boldsymbol{u}}_B(y)\mathrm{e}^{\mathrm{i}kx} + \text{c.c}$, $\rho' = \hat{\rho}_B(y)\mathrm{e}^{\mathrm{i}kx} + \text{c.c}$, onto the shear flow

$$U(y) = U_0 + \mathscr{U}\tanh(y/\delta), \quad \rho(y) = \tfrac{1}{2}(\rho_2 + \rho_1) + \tfrac{1}{2}(\rho_1 - \rho_2)\tanh(y/\delta), \tag{1.2}$$

is stretched by the shear while its intensity is reduced, a manifestation of the transfer of energy from the initial baroclinic condition to the background shear.

The goal of this study is to show how the continuous spectrum of the underlying operator is directly connected with such a damping-by-filamentation process. While *analytical* results on non-normal dynamics are somewhat hard to obtain, and only sparse findings appear in the literature, at least in the present case of continuous spectrum a more in-depth mathematical study based on systematic asymptotics analysis can be carried out. This effectively describes and predicts the evolution observed in a wide class of direct numerical simulations.

2. The continuous spectrum

In stratified parallel shear layers of inviscid fluids under the Boussinesq approximation, linear eigenmodes $\psi(x, y, t) = \hat{\psi}(y)\mathrm{e}^{\mathrm{i}k(x-ct)}$ are governed by the appropriate version of the so-called Taylor–Goldstein equation (Miles 1961)

$$(U - c)(\partial_{yy} - k^2)\hat{\psi} + \left(\frac{N^2}{U - c} - U_{yy}\right)\hat{\psi} = 0, \tag{2.1}$$

where ψ is the perturbation streamfunction, x and y are respectively the horizontal streamwise and vertical cross-flow coordinates, k and c are streamwise wavelength and

phase speed of the eigenmode, $U(y)$ is the horizontal velocity profile, and $N^2(y)$ is the squared Brunt–Väisälä frequency defined as $N^2 = -g\rho_y/\rho_0$. Here ρ_0 is the reference density scale used in the Boussinesq approximation. Variables are henceforth non-dimensionalized on the shear thickness δ, its span $\mathscr{U}$, and ρ_0. The density-perturbation eigenfunction associated with $\hat{\psi}$ is given by $\hat{\rho} = (\rho_0/g)N^2\hat{\psi}/(U-c)$. We consider flows confined between rigid plates at $y = \pm L$, where the slip-wall condition

$$\hat{\psi}(\pm L) = 0 \tag{2.2}$$

applies. We limit the present study to stable stratifications and to monotonic velocity profiles, where velocity extrema U_m and U_M are attained at the boundaries.

The problem (2.1) can be regarded as a (generalized) eigenvalue problem in either c or k, respectively assigning to k or c a fixed real value. Alternatively, the frequency $\omega \equiv c\,k$ can be fixed (real) and c eliminated from (2.1). The former and latter choices are usually referred to as the temporal and spatial spectrum respectively. In either case the Taylor–Goldstein equation can possess a discrete set of real eigenvalues, and, if the Richardson number $Ri(y) \equiv -g\rho_y/(\rho_0 U_y^2)$ is less than $1/4$ for some y, a discrete set of complex eigenvalues (Miles 1961) can also emerge. Eigenfunctions possess a critical layer at $y = y_c(c)$, defined by $U(y_c) = c$. Such a critical layer corresponds to a Frobenius (regular) singularity in the differential equation (2.1), provided $U_y(y_c) \neq 0$. If this is not the case, the local behaviour of the solution degenerates into an essential singularity, which greatly increases the analytical challenge. We shall rule out this possibility by assuming $U_y(y) \neq 0$ everywhere (a condition met in many cases of practical interest). Besides the discrete spectrum, there exists a continuous spectrum for the eigenvalue $c \in [U_m, U_M]$ (Case 1960; Dyson 1960; Banks, Drazin & Zaturska 1976). The associated eigenfunctions, here denoted by $\hat{\phi}$, must be accounted for in order to obtain a complete modal basis, which is necessary to obtain the general solution of initial value problems by eigenfunction superposition. For clarity, we denote as $\hat{\phi}_k(y, c)$ and $\hat{\phi}_\omega(y, k)$ the eigenfunctions associated with the temporal (k fixed) and spatial (ω fixed) continuous spectrum, respectively. We stress that, for the continuous spectrum in particular, the distinction between a spatial and temporal spectrum is not substantial, but rather a matter of notational convenience. In fact, any (k, ω)-pair belongs to the spectrum (i.e. it makes (2.1) solvable under the appropriate boundary conditions) provided the corresponding $c = \omega/k$ fall in the range $[U_m, U_M]$.

The spectral theory of operators in the class to which (2.1) belongs can be rather technical (see e.g. Faddeev 1971 for homogeneous shear flows). In what follows we adopt a more practical perspective. In general, continuous-spectrum eigenfunctions are obtained after weakening the conditions under which discrete-spectrum eigenfunctions are defined (for this reason the former are often referred to as generalized eigenfunctions). For instance, the Orr–Sommerfeld equation in unbounded domains possesses a continuous spectrum which is found by requiring the eigenfunctions to simply be bounded instead of decaying at (spatial) infinity (Grosch & Salwen 1978). In our case, we seek generalized eigenfunctions by enforcing the same boundary conditions as for the discrete-spectrum modes while allowing the singular point y_c to lie on the real y-axis. This is not the case for the discrete-spectrum eigenfunctions, as the corresponding eigenvalues lie outside the range of $U(y)$. In what follows we shall discuss particular solutions constructed using only eigenfunctions associated with the continuous spectrum.

2.1. *Properties of continuous-spectrum eigenfunctions*

Despite the technical difficulties associated with the formal theory of generalized eigenfunctions (Faddeev 1971), continuous-spectrum eigensolutions are relatively easy to construct for problem (2.1). This can be accomplished by patching a left- and a right-hand solution of the Taylor–Goldstein equation for fixed c in $[U_m, U_M]$ at the critical point y_c, with each solution satisfying boundary conditions on its respective side of the domain.

Solutions of (2.1) are analytic in both arguments y and c, with a branch-cut singularity at $y = y_c$, and, correspondingly, at $c = U(y)$. The functions $\hat{\phi}(y, c)$ can be expressed by Frobenius expansions in y, given by

$$\hat{\phi}(y, c, k) = (y - y_c)^{1/2+\nu} \sum_{n=0}^{+\infty} a_n (y - y_c)^n + (y - y_c)^{1/2-\nu} \sum_{n=0}^{+\infty} b_n (y - y_c)^n, \tag{2.3}$$

where the indicial exponent ν is

$$\nu(c) = (1/4 - Ri(y_c))^{1/2}. \tag{2.4}$$

For $Ri > 1/4$ we have that $a_n = b_n^*$ for $\hat{\phi}(y, c)$ to be a real-valued function of y (by factoring out a complex constant, if necessary). We also set $|a_0| = 1$ and $b_0 = \overline{a_0}$ as the normalization criterion. After noting that the singularity in c of the Taylor–Goldstein equation is removed by changing to the independent variable $z(y) = U(y) - c$, which is a smooth one-to-one mapping, it can be verified that the eigenfunctions have the structure

$$\hat{\phi}(y, c, k) = (y - y_c)^{1/2+\nu} \chi(y, c, k) + (y - y_c)^{1/2-\nu} \xi(y, c, k), \tag{2.5}$$

where the functions χ and ξ are entire in all arguments.

From the above expansion it is easily inferred that the corresponding pressure perturbations, $\hat{p}$ say, vanish at the critical layer. In fact, from the defining relation $\hat{p} = (U - c)\hat{\psi}_y + U_y\hat{\psi}$, we obtain that $\lim_{y \to y_c} \hat{p} = 0$ on either side of y_c, i.e. the critical layer dynamically isolates left- and right-handed solutions from each other. This fact implies lack of a dynamically motivated continuation rule across y_c, which leaves arbitrariness in patching solutions of (2.1) to obtain the continuous functions $\hat{\phi}(y, c)$. This in turn implies that, for any c inside $[U_m, U_M]$, there exists a pair of linearly independent eigenfunctions (cf. Case 1960 for a similar result by a different approach). We define right- and left-handed ϕ components by, respectively,

$$\hat{\phi}^+(y, c, k) = 0 \quad \text{for } y < y_c, \qquad \hat{\phi}^-(y, c, k) = 0 \quad \text{for } y > y_c. \tag{2.6}$$

It should be noted that, for the same reason, the expansion (2.3) is one-sided, i.e. it cannot be analytically continued around $y = y_c$ when referred to $\hat{\phi}$ solutions. We remark that a continuation rule yielding an asymptotic match between the inviscid modes and viscous-diffusive modes in the low viscosity and diffusivity limit is not needed here, even though this may be required in other cases, such as those by Booker & Bretherton (1967) and Van Duin & Kelder (1986). In fact, the continuous spectrum is in general depleted by introducing any small amount of viscosity and diffusivity, as diffusive effects remove the singular point in the governing equations, see Grosch & Salwen (1978) for a comprehensive discussion of the homogeneous ($N = 0 = Ri$) case. Note that an unbounded y-domain generically introduces a continuous spectrum (due to a singularity at infinity) in the viscous/diffusive case as well, but such

a spectral component is unrelated to the continuous spectrum $c \in [U_m, U_M]$ of the inviscid problem.

In the following it will be necessary to determine the asymptotic behaviour of the eigenfunctions close to the singularity with respect to c and k, for fixed y. Note first that the structure of the c-expansion about $c = U(y)$ does not retain the Frobenius structure of the y-expansion, because the singularity $(y - y_c)^{1/2\pm\nu}$ in (2.3) introduces logarithmic terms when this is expanded in c. The leading term of such expansions, however, consists of an algebraic singularity with the same index. The Taylor expansions in y about $y = y_c$ of $(c - U)$ and $(k - k_c)$, given by

$$\begin{aligned} c - U &= c - U(y_c) - U_y(y_c)(y - y_c) + O[(y - y_c)^2] \\ &= -U_y(y_c)(y - y_c) + O[(y - y_c)^2], \end{aligned} \tag{2.7}$$

and

$$\begin{aligned} k - k_c &= k - k_c(y_c) - \frac{\mathrm{d}k_c}{\mathrm{d}y}(y_c)(y - y_c) + O[(y - y_c)^2] \\ &= \omega \frac{U_y(y_c)}{U^2(y_c)}(y - y_c) + O[(y - y_c)^2], \end{aligned} \tag{2.8}$$

allow the conversion of y-expansions into c- and k-expansions:

$$\begin{aligned} \hat{\phi}_k^{\pm}(y, c) \sim a_0 \left(-\frac{c - U}{U_y} \right)^{1/2+\nu} + b_0 \left(-\frac{c - U}{U_y} \right)^{1/2-\nu} \\ + o[(c - U)^{1/2\pm\nu}] \quad \text{for } c \to U^{\mp} \end{aligned} \tag{2.9}$$

with $\nu = \nu(U(y))$, $U = U(y)$ and $U_y = U_y(y)$, and

$$\begin{aligned} \hat{\phi}_\omega^{\pm}(y, k) \sim a_0 \left(\frac{U^2}{\omega U_y}(k - k_c) \right)^{1/2+\nu} + b_0 \left(\frac{U^2}{\omega U_y}(k - k_c) \right)^{1/2-\nu} \\ + o[(k - k_c)^{1/2\pm\nu}] \quad \text{for } k \to {k_c}^{\pm}. \end{aligned} \tag{2.10}$$

In figure 2 a few eigenfunctions from both the continuous and the discrete spectrum are shown. Observe how the discrete-spectrum modes collapse on each other in the bulk of the shear and their oscillations localize near the boundaries. This shows how the continuous spectrum can play a dominant role in the dynamics localized around the shear core, while discrete-spectrum eigenfunctions may develop boundary layers as $Ri \to 0$ (see, e.g., Banks *et al.* 1976).

3. Continuous-spectrum solutions

For the streamfunction the superposition of continuous-spectrum eigenfunctions can be written for either left- or right-handed eigenfunctions as

$$\Phi(x, y, t) = \int_{-\infty}^{+\infty} \int_{U_m}^{U_M} H^{\pm}(k, c) \hat{\phi}^{\pm}(y, k, c) \mathrm{e}^{\mathrm{i}k(x - ct)} \, \mathrm{d}c \, \mathrm{d}k, \tag{3.1}$$

where $H^{\pm}(k, c)$ represents the coefficients of the continuous superposition, determined by specific initial conditions. (The real part is understood hereafter for all physical quantities.) The above construction gives rise to a very broad class of solutions. Amid such generality, we restrict attention to individual wave packets, here understood as distributions $H^{\pm}(k, c) = \delta(k - \kappa(s))\delta(c - \gamma(s)) \equiv W^{\pm}(s)$ localized on a path Γ specified

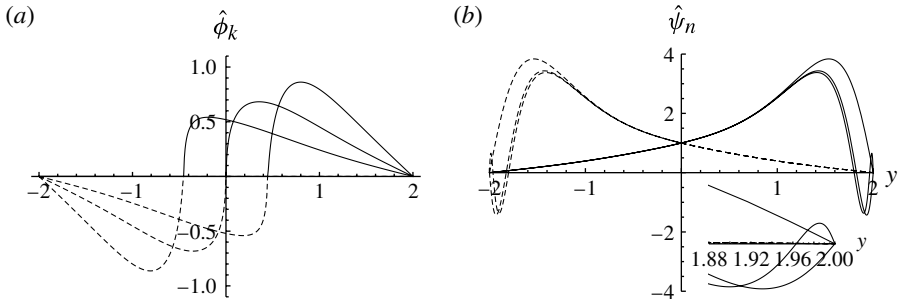

FIGURE 2. Eigenfunctions for the shear layer (1.2), with $k = 1$ and $Ri(0) = 0.35$ (real spectrum). Rigid lids placed at $y = \pm 2$. (*a*) Three pairs of continuous-spectrum modes, $\hat{\phi}^+$ (solid lines) and $\hat{\phi}^-$ (dashed lines). (*b*) First three pairs of discrete-spectrum modes, $\hat{\psi}_n$, corresponding to the three largest eigenvalues $c_n > U_M$ and the three smallest $c_n < U_m$.

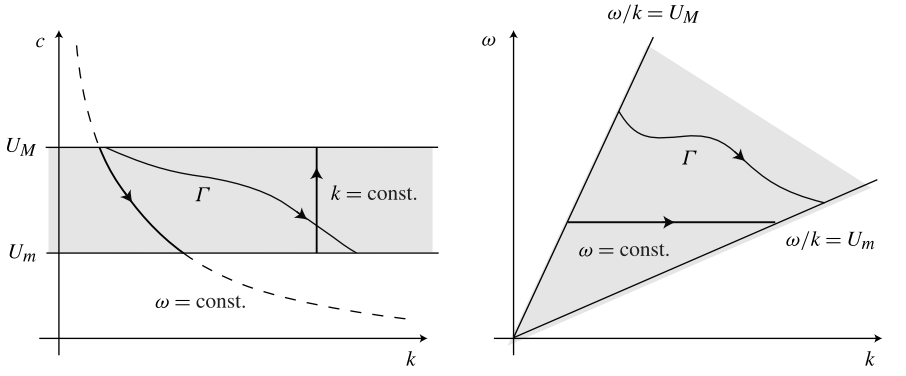

FIGURE 3. Regions in (c, k) and (ω, k) space filled by the continuous spectrum (shaded areas) and integration paths for the temporal, spatial and generic (thin Γ-curves) cases of § 3.

by the parameterized curves $\kappa(s)$ and $\gamma(s)$ in the (k, c) plane (see figure 3). In doing so, we obtain one-dimensional superpositions

$$\Phi_\Gamma = \int_\Gamma W^\pm(s)\hat{\phi}^\pm(y, \kappa(s), \gamma(s))\mathrm{e}^{\mathrm{i}\kappa(s)(x-\gamma(s)t)}\,\mathrm{d}s. \tag{3.2}$$

Note that, while the $\hat{\phi}$ are individually weak solutions of the Taylor–Goldstein equation, one can construct smooth physical solutions by superposition. This can be verified by changing the integration variable s into $\zeta(s) = y - y_c(\gamma(s))$ in (3.2). If $\gamma(s)$ is invertible, then $\zeta(s)$ is a one-to-one mapping, with $s = \gamma^{-1}[U(y - \zeta)]$ (recall the assumption of monotonic velocity profile), so that

$$\Phi_\Gamma = -\int_\Gamma W^\pm(\zeta^{1/2+\nu}\chi + \zeta^{1/2-\nu}\xi)\mathrm{e}^{\mathrm{i}\kappa(x-\gamma t)}U_y\frac{\mathrm{d}s}{\mathrm{d}\gamma}\,\mathrm{d}\zeta, \tag{3.3}$$

where each term in the integrand can only have analytic dependence on y, due the regularity of the mapping. The above integrand then depends analytically on y provided $Ri > 1/4$ everywhere, hence so does the integral Φ_Γ (see e.g. Whittaker & Watson 1927, p. 92). The same argument applies to the corresponding density field.

The arbitrariness of Γ allows the construction of wave packets possessing any dispersion relation $\omega = \omega(k)$, as shown in figure 3. If Γ is a graph with respect to k it is possible to write the above integral in the canonical form for dispersive wave packets

$$\Phi_\Gamma = \int_{k_{min}}^{k_{max}} w_\Gamma^{\pm}(k)\phi^{\pm}(y,k,c)\mathrm{e}^{\mathrm{i}(kx-\omega(k)t)}\,\mathrm{d}k, \tag{3.4}$$

with $w_\Gamma(k) = W(k, c(k))(\mathrm{d}s/\mathrm{d}k)$. In this form, the tools of asymptotic analysis for large values of x and t can be applied directly. For instance, steepest-descent analysis along the rays $x/t = \text{const.}$ for long times (Erdelyi 1956; Whitham 1974) allows a study of the asymptotic behaviour past initial transients once this dispersion relation is fixed by the path in the k, c-plane. However, it is important to realize that the peculiarities of the continuous-spectrum solutions, which account for the observations reported in the introduction, do not arise from dispersive dynamics, but rather from the singularity of the integral kernel. This can be brought forth through an asymptotic analysis based on the eigenfunction singularities. Below, we illustrate this point by focusing on two limiting cases for which the contribution of the singular kernel can be computed explicitly: the first case, which will be referred to as temporal solutions, is defined by setting k constant; the second case, referred to as spatial solutions, is defined by constant frequency ω. The corresponding paths for these limiting cases are shown in figure 3.

3.1. *Temporal solutions*

In the first case, $k = \text{const.}$, solutions for both streamfunction and density are written as

$$\Phi_k(x,y,t) = \hat{\Phi}_k(y,t)\mathrm{e}^{\mathrm{i}kx}, \quad R_k(x,y,t) = \hat{R}_k(y,t)\mathrm{e}^{\mathrm{i}kx}, \tag{3.5}$$

with

$$\hat{\Phi}_k = \int_{U_m}^{U_M} \hat{\phi}_k^{\pm} w_k^{\pm}\mathrm{e}^{-\mathrm{i}kct}\,\mathrm{d}c, \quad \hat{R}_k = \int_{U_m}^{U_M} \hat{\rho}_k^{\pm} w_k^{\pm}\mathrm{e}^{-\mathrm{i}kct}\,\mathrm{d}c, \tag{3.6}$$

where $w_k^{\pm}(c;k)$ are the coefficients of the linear superposition.

To begin with, notice that for long times, $|kt| \gg 1$ (recall the non-dimensionalization introduced in § 2), the exponential term inside the integrals (3.6) becomes highly oscillatory. Under the sole assumption that $w^{\pm}(c;k)$ are integrable functions of $c \in [U_m, U_M]$, the Riemann–Lebesgue lemma ensures that

$$\lim_{|t|\to\infty} \hat{\Phi}_k(y,t) = \lim_{|t|\to\infty} \hat{R}_k(y,t) = 0 \tag{3.7}$$

for any fixed y. We require that $w^{\pm}(c;k)$ is analytic in c and that $w^{\pm} \to 0$ as $c \to (U_m, U_M)$ sufficiently fast. In this case the dominant contribution to the integral localizes around $c = U(y_c)$, the branch-point singularity of $\hat{\phi}$, so that the asymptotic decay rate is dictated by the leading term in the Frobenius expansion (2.3). For general shear flows the long-time asymptotic expansion of (3.6) can be obtained by applying Watson's lemma (see e.g. Erdelyi 1956). Thus, the long-time asymptotic expansion

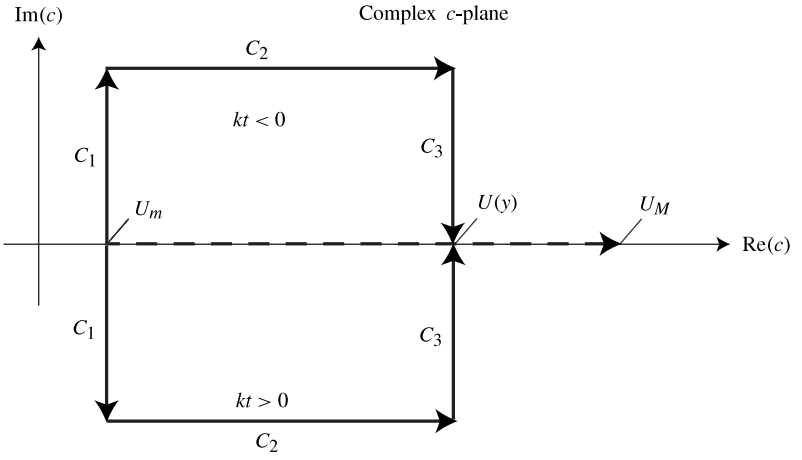

FIGURE 4. Path of integration in the complex plane for $\hat{\phi}^+$-mode temporal solutions.

of an integral of the form $I(t) = \int_0^b f(x)\mathrm{e}^{-xt}\,\mathrm{d}x$ is $I \sim \sum a_0\Gamma(\alpha+\beta n+1)t^{-\alpha-\beta n-1}$, provided f possesses the expansion $f = \sum_0^N a_0 x^{\alpha+\beta n} + o(x^{\alpha+\beta N})$ about $x = 0$ and is smooth elsewhere. In order to apply this result to the integrals in (3.6), we first deform the integration path away from the real axis into the complex plane, as illustrated in figure 4. With reference to this sketch and $kt > 0$, say, the contributions from the segments C_1 and C_2 are asymptotically subdominant: on C_2 the integrand is uniformly exponentially small, $O(\mathrm{e}^{-k|C_1|t})$ (where $|C_n| > 0$ is the length of C_n), while on C_1 the leading contribution comes from the upper extremum ($c = U_M$) where the integrand has (at most) a simple zero. Along C_3, in contrast, upon the variable transformation $-\mathrm{i}\ell = (c - U(y))$ the first integral in (3.6) (the other can be treated similarly) becomes a canonical Watson integral:

$$\mathrm{i}\int_0^{|C_3|}\hat{\phi}_k^{\pm}w_k^{\pm}\mathrm{e}^{-k\ell t}\,\mathrm{d}\ell \sim \mathrm{e}^{-\mathrm{i}kUt}\,\mathrm{i}\int_0^{|C_3|}\left[a_0\left(\frac{\mathrm{i}\ell}{U_y}\right)^{1/2+\nu} + b_0\left(\frac{\mathrm{i}\ell}{U_y}\right)^{1/2-\nu}\right]\overline{w}_k^{\pm}\mathrm{e}^{-k\ell t}\,\mathrm{d}\ell. \quad (3.8)$$

This procedure yields the long-time $kt \to +\infty$ solution

$$\hat{\Phi}_k = A\mathrm{e}^{-\mathrm{i}kUt}\,(kt)^{-3/2+\nu} + B\mathrm{e}^{-\mathrm{i}kUt}\,(kt)^{-3/2-\nu} + o[(kt)^{-3/2\pm\nu}], \quad (3.9a)$$

$$\hat{R}_k = C\mathrm{e}^{-\mathrm{i}kUt}\,(kt)^{-1/2+\nu} + D\mathrm{e}^{-\mathrm{i}kUt}\,(kt)^{-1/2-\nu} + o[(kt)^{-1/2\pm\nu}], \quad (3.9b)$$

where the multipliers $A, \ldots, D$, defining $\overline{w}^{\pm} = w^{\pm}(U(y))$, are

$$A = a_0\mathrm{i}\left(\frac{\mathrm{i}}{U_y}\right)^{1/2+\nu}\overline{w}^{\pm}\Gamma\left(\frac{3}{2}+\nu\right), \quad B = b_0\mathrm{i}\left(\frac{\mathrm{i}}{U_y}\right)^{1/2-\nu}\overline{w}^{\pm}\Gamma\left(\frac{3}{2}-\nu\right), \quad (3.10a)$$

$$C = -\rho_y\left(\frac{1}{2}+\nu\right)^{-1}\mathrm{e}^{\mathrm{i}\pi/2}A, \qquad D = -\rho_y\left(\frac{1}{2}-\nu\right)^{-1}\mathrm{e}^{\mathrm{i}\pi/2}B. \quad (3.10b)$$

Note that the above expressions hold for $kt \to -\infty$ after taking the complex conjugate due to the Hermitian symmetry of the Fourier transform.

The above formulae reveal the physical structure of the continuous-spectrum superposition under study, (3.6). On each horizontal section ($y = \text{const.}$) the solution consists of a wave travelling at the local flow speed with amplitude changing in time, either growing ($t < 0$) or decaying ($t > 0$). Such behaviour is qualitatively that of the exact solution for a linear background, though featuring non-uniform stretching and decay rate. In fact, setting $w^{\pm} = \exp(\mathrm{i}lc)$, the above formulae recover a result known for linearly stratified shears, $U(y) = y$ and $N^2 = \text{const.}$ (see e.g. Farrel & Ioannou 1993), whose derivation has so far been crucially linked to the specific linear stratification setup.

3.2. *Spatial solutions*

In considering solutions consisting of constant (real) frequency ω, distinction should be made between the cases in which the shear profile $U(y)$ is sign-definite and when it is not. In the first case k varies within $[\omega/U_M, \omega/U_m]$, while in the second case it takes values in the open intervals $[\omega/U_M, \infty)$ and $(-\infty, \omega/U_m]$. We limit ourselves to the simpler (sign-definite) first case, leaving the more lengthy discussion of the second case to future work. Note that $\omega = \text{const.}$ implies zero group velocity $c_g \equiv \mathrm{d}\omega/\mathrm{d}k$, which can then be shifted to any constant by Galilean transformation. Hence, the above distinction between the sign of $U(y)$ being definite or not, translates into c_g lying outside or inside the range of U.

Spatial time-periodic solutions for the first case are

$$\Phi_\omega(x, y, t) = \hat{\Phi}_\omega(x, y)\mathrm{e}^{-\mathrm{i}\omega t}, \quad R_\omega(x, y, t) = \hat{R}_\omega(x, y)\mathrm{e}^{-\mathrm{i}\omega t}, \tag{3.11}$$

with

$$\hat{\Phi}_\omega = \int_{\omega/U_M}^{\omega/U_m} \hat{\phi}_\omega^{\pm} w_\omega^{\pm} \mathrm{e}^{\mathrm{i}kx}\,\mathrm{d}k\,, \quad \hat{R}_\omega = \int_{\omega/U_M}^{\omega/U_m} \hat{\rho}_\omega^{\pm} w_\omega^{\pm} \mathrm{e}^{-\mathrm{i}kx}\,\mathrm{d}k. \tag{3.12}$$

The same analysis as for the $\hat{\Phi}_k$ solutions yields results analogous to (3.9) for the time-periodic case, i.e. the far-field $x \to +\infty$ solution

$$\hat{\Phi}_\omega = A\mathrm{e}^{\mathrm{i}k_c x} x^{-3/2+\nu} + B\mathrm{e}^{\mathrm{i}k_c x} x^{-3/2-\nu} + o(x^{-3/2\pm\nu}), \tag{3.13a}$$

$$\hat{R}_\omega = C\mathrm{e}^{\mathrm{i}k_c x} x^{-1/2+\nu} + D\mathrm{e}^{\mathrm{i}k_c x} x^{-1/2-\nu} + o(x^{-1/2\pm\nu}), \tag{3.13b}$$

where the multipliers $A, \ldots, D$, defining $\overline{w}^{\pm} = w^{\pm}(k_c)$, are

$$A = a_0\mathrm{i}\left(\frac{\mathrm{i}U^2}{\omega U_y}\right)^{1/2+\nu} \overline{w}^{\pm}\Gamma\left(\frac{3}{2}+\nu\right), \quad B = b_0\mathrm{i}\left(\frac{\mathrm{i}U^2}{\omega U_y}\right)^{1/2+\nu} \overline{w}^{\pm}\Gamma\left(\frac{3}{2}+\nu\right), \tag{3.14a}$$

$$C = -\rho_y\frac{\omega}{U^2}\left(\frac{1}{2}+\nu\right)^{-1}\mathrm{e}^{-\mathrm{i}\pi/2}A, \qquad D = -\rho_y\frac{\omega}{U^2}\left(\frac{1}{2}+\nu\right)^{-1}\mathrm{e}^{-\mathrm{i}\pi/2}B. \tag{3.14b}$$

Once again, for $x \to -\infty$ the complex conjugate of the above expressions must be taken.

The continuous-spectrum solutions are constructed numerically by discretizing the vertical coordinate in a uniform grid of points, y_n, and defining a corresponding set of discrete values $c_n = U(y_n)$, $n = 1, 2, \ldots, N_c$ (or $k_n = \omega/U(y_n)$ in the spatial case). For any index n the eigenfunctions can be computed by solving the Taylor–Goldstein equation with an ODE solver package. The numerical integration is started from a boundary (upper for $\hat{\phi}^+$, lower for $\hat{\phi}^-$) and terminated close to the singular point y_c. Attention must be paid in order to ensure accuracy when approaching y_c (current

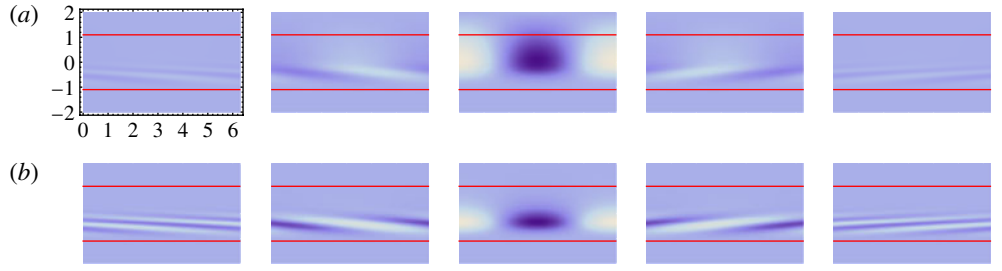

FIGURE 5. Time frames of a temporal solution, Φ_k (a) and R_k (b), for $k = 1$, $w^+ = \exp[-8\,(y_c + 1/2)^2]$, $w^- = 0$. Frames are taken at instants $t = -20, -10, 0, 10, 20$. Horizontal lines reference the same level of mean background density as in figure 1.

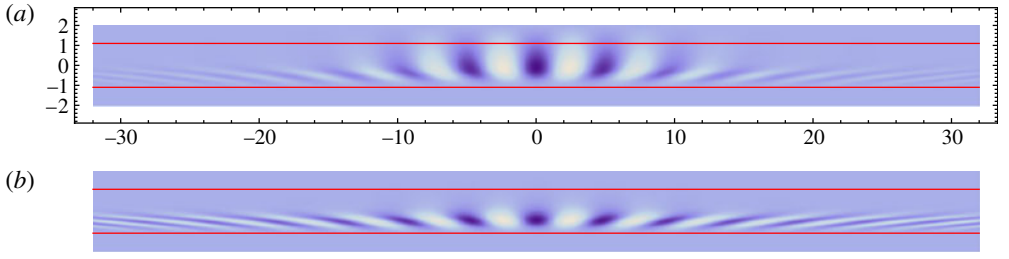

FIGURE 6. Spatial solution, Φ_ω (a) and R_ω (b), at $t = 0$ for $\omega = 2$, $w^+(k) = \exp[-8\,(y_c(\omega/k) + 1/2)^2]$, $w^- = 0$. Horizontal lines reference the same level of mean background density as in figure 1.

software packages provide very accurate adaptive solvers that can accomplish this result with limited efforts). The integrals in (3.6) and (3.12) are then accurately approximated by combining a trapezoid rule away from the singularity with an exact integration of the appropriate local expansion, (2.9) or (2.10), in a small neighbourhood of the singular point.

In what follows, we set $N_c = 385$. The examples we present refer to the background flow (1.2), with $U_0 = 2$, $\mathscr{U} = 1$, $\rho_1 = 0.966$ and $\rho_2 = 1.034$, $\delta = 1$. The corresponding overall Richardson number is $Ri(0) = 0.35$ (stable shear). The vertical domain extent is set to $L = 2$. The temporal solution is visualized in figure 5. The orientation of the filaments in the shear determines whether compression or stretching occurs. As compressing filaments are eventually overturned by the shear, their growth cannot proceed indefinitely and is only observable in transients. A comparison between figures 1 and 5 indicates that the continuous spectrum dominates the evolution in the direct numerical simulation example presented in the introduction (note the reversal of filament orientation reflecting the opposite sign of the shear in the example). Figure 6 contains the corresponding spatial solution. The figure shows the same mechanism of increase/decrease associated with compression/stretching of the perturbations found in

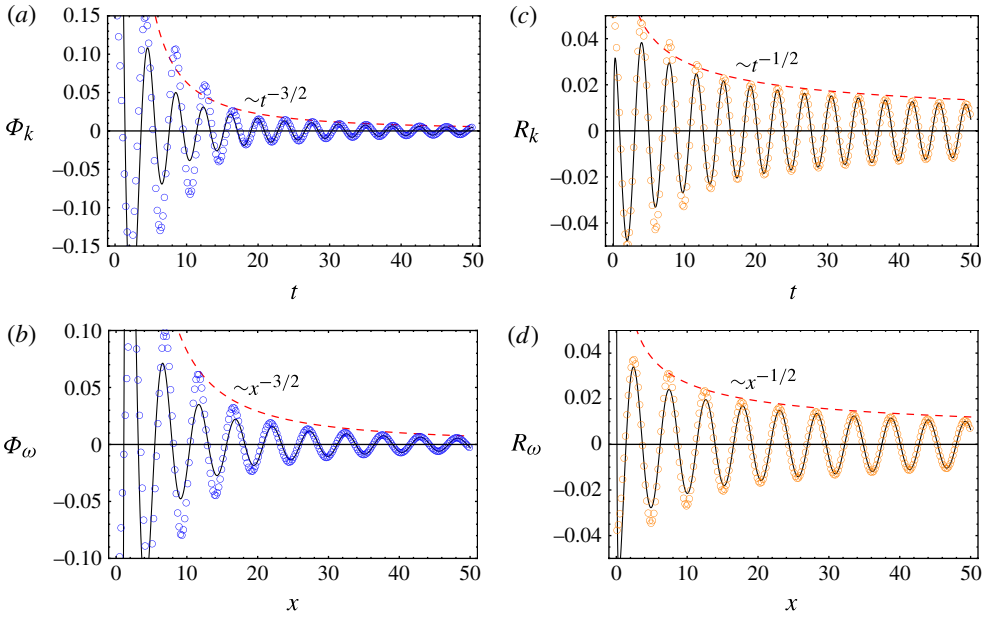

FIGURE 7. Continuous-spectrum solutions and corresponding asymptotic expansions. (*a*,*c*) Temporal slice of the solution depicted in figure 5 (symbols) and asymptotic formula (3.9) (solid line) at $x = 0$ and $y = -0.335$ (roughly the level containing the most intense fluctuations). (*b*,*d*) Horizontal slice of the solution depicted in figure 6 (symbols) and asymptotic formula (3.13) (solid line) taken at $y = -0.335$. Asymptotic trends are referenced by the dashed lines.

the temporal solution, with evolution now taking place in space. The above asymptotic analysis is compared to the 'exact' numerical solutions in figure 7. This shows the agreement with the full solutions of the asymptotic approximations for large times and distances in their respective cases.

4. Conclusions

We have presented and analysed by means of rigorous asymptotic methods a new class of exact solutions for linearized perturbations in stratified parallel shear flows. Such solutions generalize a previous exact result (Farrel & Ioannou 1993) to general shear profiles, and, perhaps most notably, include its spatial analogue. These results provide new physical information on the role of the continuous spectrum in stratified shear flows. In particular, we have shown how the continuous spectrum is connected to a reversible mechanism of enhancement-by-compression, which naturally converts into damping-by-filamentation after the shear overturns the perturbation structures. This justifies the transient nature of non-normal growth. The physical features illustrated through specific examples are robust (i.e. they hold for a wide class of shear profiles and initial perturbations) as they follow from the mathematical structure of continuous-spectrum eigenfunctions, and this is essentially independent of setup details.

From a broader viewpoint, these results provide a theoretical underpinning to the observations reported for non-parallel shear flows in Camassa & Viotti (2012). Together, these studies suggest that non-normal dynamics can have a significant impact

on the onset of instability. Its interplay with other effects, such as Kelvin–Helmholtz waves, should be accounted for, which in this context appears to have been largely ignored so far.

In closing, it is interesting to note that the present analysis can be extended to other types of flow, whenever the underlying stability operator shares a similar structure. A notable example is provided by compressible swirling flows; indeed, our main findings hold consistently with algebraic far-field solutions and non-normal effects observed in such a context, see Heaton & Peake (2006).

Acknowledgements

This research is supported by NSF grants DMS-0509423, DMS-1009750 and RTG DMS-0943851. The authors wish to thank A. Almgren for providing and helping with the numerical code VARDEN, and D. Adalsteinsson for help with his software package DataTank. The authors also wish to express gratitude to an anonymous referee for bringing to their attention the interesting spectral property connections between stratified and swirling flows.

References

ALMGREN, A. S., BELL, J. B., COLELLA, P., HOWELL, L. H. & WELCOME, M. L. 1998 A conservative adaptive projection method for the variable density incompressible Navier–Stokes equations. *J. Comput. Phys.* **142**, 1–46.

BANKS, W. H. H., DRAZIN, P. G. & ZATURSKA, M. B. 1976 On the normal modes of parallel flow of inviscid stratified fluid. *J. Fluid Mech.* **75**, 149–171.

BOOKER, J. R. & BRETHERTON, F. P. 1967 The critical layer for internal gravity waves in a shear flow. *J. Fluid Mech.* **27**, 513–539.

CAMASSA, R. & VIOTTI, C 2012 On the response of large-amplitude internal waves to upstream disturbances. *J. Fluid Mech.* **702**, 59–88.

CASE, K. M. 1960 Stability of an idealized atmosphere. I. Discussion of results. *Phys. Fluids* **3**, 149–154.

DYSON, F. J. 1960 Stability of an idealized atmosphere. II. Zeros of the confluent hypergeometric function. *Phys. Fluids* **3**, 155–157.

ERDELYI, A. 1956 *Asymptotic Expansions*. Dover.

FADDEEV, L. D. 1971 On the theory of the stability of stationary plane-parallel flows of an ideal fluid. *Zap. Nauchn. Sem. Leningrad Otdel. Mat. Inst.* **21**, 164–172.

FARREL, B. F. & IOANNOU, P. J. 1993 Transient development of perturbations in stratified shear flows. *J. Atmos. Sci.* **50**, 2201–2214.

GROSCH, C. E. & SALWEN, A. 1978 The continuous spectrum of the Orr–Sommerfeld equation. Part 1. The spectrum and the eigenfunctions. *J. Fluid Mech.* **87**, 33–54.

HEATON, C. J. & PEAKE, N. 2006 Algebraic and exponential instability of inviscid swirling flow. *J. Fluid Mech.* **565**, 279–318.

MILES, J. W. 1961 On the stability of heterogeneous shear flows. Part 1. *J. Fluid Mech.* **10**, 496–508.

VAN DUIN, C. A. & KELDER, H. 1986 Internal gravity waves in shear flows at large Reynolds number. *J. Fluid Mech.* **169**, 293–306.

WHITHAM, G. B. 1974 *Linear and Nonlinear Waves*. Wiley.

WHITTAKER, E. T. & WATSON, G. N. 1927 *A Course of Modern Analysis*. Cambridge University Press.